THE JOURNAL OF BIOLOGICAL CHEMISTRY VOL. 291, NO. 2, pp. 739–751, January 8, 2016
© 2016 by The American Society for Biochemistry and Molecular Biology, Inc. Published in the U.S.A.

Amyloid Assemblies of Influenza A Virus PB1-F2 Protein Damage Membrane and Induce Cytotoxicity*

Received for publication, October 27, 2015, and in revised form, November 17, 2015 Published, JBC Papers in Press, November 24, 2015, DOI 10.1074/jbc.M115.652917

Jasmina Vidic[‡1], **Charles-Adrien Richard**[‡], **Christine Péchoux**[§], **Bruno Da Costa**[‡], **Nicolas Bertho**[‡], **Sandra Mazerat**[¶], **Bernard Delmas**[‡], **and Christophe Chevalier**[‡]

From the [‡]*Unité de Virologie et Immunologie Moléculaires, INRA, UR892, Domaine de Vilvert, 78350 Jouy en Josas, the* [§]*Génétique Animale et Biologie Intégrative, INRA, UMR1313, Domaine de Vilvert, 78350 Jouy en Josas, and the* [¶]*Institut de Chimie Moléculaire et des Matériaux d'Orsay, Université Paris-Sud, CNRS, UMR 8182, 91400 Orsay, France*

PB1-F2 is a small accessory protein encoded by an alternative open reading frame in PB1 segments of most influenza A virus. PB1-F2 is involved in virulence by inducing mitochondria-mediated immune cells apoptosis, increasing inflammation, and enhancing predisposition to secondary bacterial infections. Using biophysical approaches we characterized membrane disruptive activity of the full-length PB1-F2 (90 amino acids), its N-terminal domain (52 amino acids), expressed by currently circulating H1N1 viruses, and its C-terminal domain (38 amino acids). Both full-length and N-terminal domain of PB1-F2 are soluble at pH values ≤6, whereas the C-terminal fragment was found soluble only at pH ≤ 3. All three peptides are intrinsically disordered. At pH ≥ 7, the C-terminal part of PB1-F2 spontaneously switches to amyloid oligomers, whereas full-length and the N-terminal domain of PB1-F2 aggregate to amorphous structures. When incubated with anionic liposomes at pH 5, full-length and the C-terminal part of PB1-F2 assemble into amyloid structures and disrupt membrane at nanomolar concentrations. PB1-F2 and its C-terminal exhibit no significant antimicrobial activity. When added in the culture medium of mammalian cells, PB1-F2 amorphous aggregates show no cytotoxicity, whereas PB1-F2 pre-assembled into amyloid oligomers or fragmented nanoscaled fibrils was highly cytotoxic. Furthermore, the formation of PB1-F2 amyloid oligomers in infected cells was directly reflected by membrane disruption and cell death as observed in U937 and A549 cells. Altogether our results demonstrate that membrane-lytic activity of PB1-F2 is closely linked to supramolecular organization of the protein.

Influenza is a respiratory infection disease caused by influenza A viruses (IAVs)[2] of the *Orthomyxoviridae* family (1). The genome of IAVs is constituted by 8 segments of negative-strand RNA that encode at least 17 polypeptides (2–6). The determinism of IAV-mediated pathogenicity is complex and involves several viral proteins as HA, PB1, NS1, PA-X, and PB1-F2.

PB1-F2 is translated from an alternative +1 open reading frame of the PB1 segment (7). This small accessory protein of 87–90 amino acids displays a strong polymorphism and is expressed in most avian IAV strains (8). PB1-F2 is suspected to contribute to excessive host inflammatory response contributing to influenza severity, especially with highly pathogenic strains such as avian H5N1 or the 1918 "Spanish flu" strains (9–11). Interestingly, nowadays most human H1N1 expressed C-terminal truncated forms of the PB1-F2 (12). PB1-F2 was first described as a proapoptotic protein that down-regulates host immune response against IAV infection (7). Presumably, PB1-F2 localizes to mitochondria, induces apoptosis, and affects the mitochondria-mediated immune response (7, 13–16). Recently PB1-F2 was reported to translocate into the mitochondrial inner membrane via Tom40 channels, to accumulate within the organelle, and impair cellular innate immunity (15). Synthetic PB1-F2 protein was shown to incorporate mitochondrial membrane by direct interaction with charged lipid head groups (13). The membrane-bound PB1-B2 was supposed to self-assemble within the lipid bilayer and form non-selective pores (17, 18). Ion leakage through the PB1-F2-mediated pores break out the integrity in the planar lipid membrane (18). Likewise, PB1-F2 can disturb the inner membrane of mitochondria, which induces apoptosis. Other functions of PB1-F2 have been also reported: PB1-F2 co-localizes in the nucleus of infected epithelial cells and up-regulates viral polymerase activity (19, 20); PB1-F2 may be implicated in inflammation and can modify the host pro-inflammatory response induced by IAV infection (11, 21, 22); PB1-F2 may inhibit the IFN pathway induction through interacting with the mitochondrial antiviral signaling protein, MAVS (23, 24); PB1-F2 was also shown to enhance the predisposition to secondary bacterial infection (11, 25, 26).

PB1-F2 is deprived of any ordered structure in aqueous solutions but can switch to α-helical or β-sheet secondary structures depending on hydrophobicity of the environment (12, 27). Spectroscopic analyses revealed the presence of α-helical structures within PB1-F2 only in the concentrated TFE solution, which is far from physiological conditions. In the membrane mimic environment, PB1-F2 was demonstrated to aggregate to amyloid-like structures with a characteristic amyloidal cross-β-sheet secondary structure (27–29). Additionally, PB1-F2 can adopt β-sheet conformation and oligomerize to amyloid structures within infected cells, as shown for IAV-infected monocytes and epithelial cells (27, 28).

To further understand the interaction of PB1-F2 with cellular membranes, we investigated PB1-F2 domains involved in

* The authors declare that they have no conflicts of interest with the contents of this article.

[1] To whom correspondence should be addressed. Tel.: 33-134-652623; Fax: 33-134652621; E-mail: jasmina.vidic@jouy.inra.fr.

[2] The abbreviations used are: IAV, influenza A virus; PS, phosphatidylserine; PC, phosphatidylcholine; LUV, large unilamellar liposome; DLS, dynamic light scattering; MTT, 3-(4,5-dimethylthiazol-2-yl)-2,5-diphenyltetrazolium bromide; ThT, thioflavin T.

binding to membrane bilayers and characterized the PB1-F2 conformational change and self-association occurring upon membrane binding. We demonstrate that cytotoxicity of PB1-F2 from extracellular medium strongly depends on protein structural organization. Finally, we showed that lytic activity of PB1-F2 assembled into amyloid structures contributes to cell membrane damaging upon IAV infection.

Experimental Procedures

PB1-F2 Expression and Purification—PB1-F2 protein of A/WSN/1933 (H1N1) influenza virus was expressed and purified as described previously (27). Briefly, the gene encoding either the full-length PB1-F2(1–90) protein or N-terminal domain of PB1-F2(1–52) (Nter) were cloned into the pET 22b+ expression vector (Novagen) to express His_6-tagged protein versions. Transformed competent BL-21 Rosetta cells (Stratagene) were incubated with 1 mM isopropyl 1-thio-B-D-galactopyranoside for 4 h at 37 °C. After cell lysis and solubilization in 8 M urea buffer, the recombinant PB1-F2-His proteins were purified from inclusion bodies on a Hitrap-IMAC column using the AKTA Purifier-100 FPLC chromatographic system (GE Healthcare). Fractions collected containing PB1-F2-His proteins were further purified by size exclusion chromatography on a 120-ml Sepharose Superdex 200 column. Urea was removed on a G25 desalting column equilibrated with 5 mM ammonium acetate buffer (pH 5). PB1-F2-His proteins were lyophilized and stored at −20 °C. The C-terminal domain of PB1-F2(53–90) (pCter) was custom made by Proteogenix (France). Prior to analysis lyophilized protein powder was dissolved in adequate buffer and its concentration was determined by measuring optical density at 280 nm using extinction coefficient deduced from its composition of 28,990, 5,500, and 4,833 M^{-1} cm^{-1} for PB1-F2(1–90), PB1-F2(1–52), and PB1-F2(53–90), respectively.

Reagents—Phosphatidylserine (PS) and phosphatidylcholine (PC) were purchased from Avanti Polar Lipids (AL). Sodium acetate buffers (pH 3–6), phosphate buffers (pH 7–10), and triethylammonium acetate (pH 5) were of analytical grade. Reagents for SDS-PAGE electrophoresis were obtained from Invitrogen (France). Other reagents were purchased from Sigma (France).

Liposomes Preparation—Lipids (10 mg) were solubilized in chloroform and their dry films were obtained by chloroform evaporation under a stream of nitrogen. The lipid film was then hydrated with 10 ml of 5 mM sodium acetate buffer (pH 5), and gently vortex and sonicated for a few minutes. The liposomes formed were freeze/thawed three times in liquid nitrogen (vortex between every defrosting) and subsequently extruded through a polycarbonate membrane filter (MILLIPORE 0.1 μm) to obtain large unilamellar liposomes (LUVs) of 100-nm diameter.

Liposome Permeabilization Assay—For the leakage measurements, solid lipid films were hydrated with a 10 mM sodium acetate buffer (pH 5) containing 35 mM calcein (calcein disodium salt, Fluka). After three freeze/thaw cycles, the suspensions were extruded as described above. Non-entrapped dye was removed by gel filtration on a Sephadex G-25 column (GE Healthcare) equilibrated with 10 mM sodium acetate buffer (pH 5). Calcein efflux measurements were performed on a Tecan microplate reader. The ability of different PB1-F2 proteins to permeabilize liposomes was monitored by the decrease in fluorescent intensity after the addition of proteins at the desired concentration to a 160-μl suspension of 0.01 mg/ml of liposomes in the sodium acetate buffer containing Co^{2+} ions (quencher). Calcein fluorescence emission at 528 nm was recorded continuously upon excitation 492 nm. To normalize the fluorescence intensity, the maximum quenching was obtained by the addition of 0.1% (v/v) Triton X-100. All runs were done at least in triplicate and were found to be in close agreement.

Ultracentrifugation Assay for Membrane Binding of PB1-F2—An aliquot of liposomes (0.5 mg/ml) of different lipid compositions was incubated with PB1-F2 (10 μM) in 10 mM sodium acetate buffer (pH 5) for 24 h at 4 °C. Vesicles were pelleted by centrifugation at 40,000 × *g* for 40 min at 4 °C (Beckman TL-100). The supernatant and pellets were separated and assayed for PB1-F2 by SDS-PAGE analysis and Coomassie Blue gel staining.

Circular Dichroism Spectroscopy—Far-UV (180–260 nm) circular dichroism (CD) spectra were measured on a JASCO J-810 spectropolarimeter using 1-mm path length quartz cell. Spectra were collected at a scanning rate of 100 nm/min, with a bandwidth of 1.0 nm and a resolution of 100 mdeg, and corrected for the contribution of the buffer. Measurements were done at 20 °C. Each spectrum was an average of 8–16 scans. CD spectra were analyzed and quantified using the DicroWeb software.

DLS Analysis—Dynamic light scattering (DLS) measurements were performed on a Nano series Zetasizer (Malvern, UK) using a helium-neon laser wavelength of 633 nm and detection angle of 173°. The scattering intensity data were processed using the instrumental software to obtain the hydrodynamic diameter (R_H) and the size distribution of particles in each sample. R_H of the particles was estimated from the autocorrelation function, using the Cumulants method. A total of 10 scans with an overall duration of 5 min were obtained for each sample. All measurements were done at 20 °C.

Antimicrobial Activity Assay—*Escherichia coli* strain BL21 (DE3) (Invitrogen, France) and *Bacillus subtilis* 168 strain (kindly supplied by Sandrine Auger, INRA, France) were grown overnight at 37 °C in 50 ml of Luria broth (LB) without antibiotics. The saturated cultures were diluted in fresh LB medium to reach an absorbance of 0.1 at 600 nm. Disposable sterile spectroscopic cuvettes were used to set up the experimental conditions in triplicate with each condition. 150 μl of various concentrations of the full-length or C-terminal PB1-F2 in PBS (pH 7.4) was added into the cuvette, before the addition of 700 μl of bacterial cell suspension (850 μl total volumes). Final monomer equivalent PB1-F2 concentrations were 0.5, 1, 5, and 20 μM. In mocks the protein solutions were replaced with PBS to account for the dilution of LB. All assays were performed in triplicate. After setting up cuvettes, an initial absorbance reading at 600 nm was recorded after which cuvettes were placed in a 37 °C incubator and removed at 30 min, 1 h 30, 2 h, 3 h, 4 h, and 24 h for absorbance readings.

Cell Cultures—A549 cells (human alveolar epithelial cells, American Type Culture Collection) were routinely cultured in minimal essential medium (MEM; Sigma) containing 0.2% $NaHCO_3$ (Sigma), MEM amino acids (Gibco), MEM vitamins (Gibco), 2 ml of glutamine, 100 IU/ml of penicillin, 100 μg ml^{-1} of streptomycin, and 10% fetal bovine serum. The human promonocytic cell line U937 purchased from the American Type Culture Collection (Manassas, VA) was propagated and maintained in RPMI 1640 medium (Lonza) supplemented with 10% fetal bovine serum, 2 mM L-glutamine, 100 IU/ml of penicillin, and 100 μg/ml of streptomycin, according to the American Type Culture Collection recommendations. Cells were maintained at 37 °C in a 5% CO_2 incubator.

Cell Incubation with PB1-F2 Aggregates—A549 cells were plated at a density of 30,000 cells per well on 96-well plates in 100 μl of fresh medium. After 24 h completed medium was exchanged with 100 μl of MEM without serum. Aliquots of solutions containing amyloid or non-amyloid protein aggregates formed in PBS buffer (pH 7.4) were added to the cell media at 0.1–20 μM final concentrations (monomer unit equivalents). After 24 h incubation, 20 μl of a freshly prepared stock MTT solution in PBS was added to the cells (MTT final concentration, 0.8 mg/ml) and incubated for a further 1 h. Then, the cell layer was dried and MTT formazan was suspended in 100 μl of dimethyl sulfoxide. Absorbance values were assessed at 560 nm and corrected for a background signal by subtracting the signal measured at 670 nm. Cell survival was quantified and expressed as % of cells treated only with PBS (mock).

Viral Infection and Cytometry—For infections, A549 and U937 cells were washed with serum-free medium and incubated with wild-type A/WSN/1933 (H1N1) virus or the virus knocked out for PB1-F2 expression (ΔF2) at 1 multiplicity of infection for 1 h at 37 °C. Infected cells were then incubated at 37 °C in complete medium until collection. Cell death was quantified by acridine orange followed by cytometry analysis (BD LSRFortessa, BD Bioscience) with the 488-nm laser line and the FITC (530/30) channel. Cell death was quantified by acridine orange followed by cytometry analysis (BD LSRFortessa, BD Bioscience, USA) with the 488-nm laser line and the FITC (530/30) channel. Collected cells were washed two times in PBS, then resuspended in MEM containing acridine orange (0.1 μg/ml) and incubated for 10 min in the dark. Stained cells were collected, washed two times with PBS, and then fixed with 3.5% paraformaldehyde in PBS for 30 min. For analysis, the fixed cells were collected and resuspended in PBS.

Optical Microscopy—For microscopy observations, A459 cells incubated overnight with different aggregated PB1-F2 preparations were fixed with 4% paraformaldehyde in PBS. Cells were observed with an Axio Observer fluorescence microscope (Carl Zeiss, Oberkochen, Germany) using a ×40 objective. Images were acquired and processed using AxioVision software (Carl Zeiss).

Electron Microscopy—To investigate the interaction between lipid vesicles and PB1-F2, negatively charged asolectin liposomes (0.1 mg/ml of total lipids) were prepared in 10 mM sodium acetate buffer (pH 5). Liposomes were incubated with 50 μM full-length PB1-F2 at room temperature for 5 min. Then, 10 μl of the lipid-protein sample were adsorbed onto formvar/carbon-coated 200-mesh copper grids (Agar Scientific). After deposition of the suspension, grids were washed twice for 1 min with PBS, and negatively stained by floating on a 10-μl drop of 2% (w/v) uranyl acetate (Sigma) for 1 min. The grids were air-dried before observation under a Philips EM12 electron microscope at 80 kV exciting voltage.

To visualize IAV-infected cells, U937 cells were infected with wild-type or ΔF2 virus at 5 multiplicity of infection for 1 h at 37 °C and harvested 24 h post-infection. Cultured cells were fixed with 2% glutaraldehyde in 0.1 M sodium cacodylate buffer (pH 7.2) for 1 h at room temperature. Samples were then contrasted with 0.5% Oolong Tea Extract in sodium cacodylate buffer and post-fixed with 1% osmium tetroxide containing 1.5% potassium cyanoferrate, gradually dehydrated in ethanol (30 to 100%), and substituted gradually in a mixture of propylene oxide-epon and embedded in Epon (Delta Microscopy, Labège, France). Thin sections (70 nm) were collected onto 200-mesh cooper grids, and conterstained with lead citrate. Grids were examined with Hitachi HT7700 electron microscope operated at 80 kV (Elexience, France). Images were acquired with a charge-coupled device camera (AMT).

AFM—A commercial dimension 3100 AFM (Vecco Instruments) was used for topographical characterization of the samples. All measurements were performed at the tapping mode using a rectangular silicon AFM tip.

Statistics—Data are presented as mean ± S.D. of at least three separate experiments and statistical analyses were performed using the unpaired Student's *t* test. Analyses were done with GraphPad Prism software (GraphPad, La Jolla, CA). The significance level was defined as: *, $p < 0.05$; **, $p < 0.01$; and ***, $p < 0.001$.

Results

Effect of pH on Aggregation of PB1-F2—We first sought to determine the aggregation state and secondary structure of PB1-F2 at various pH values. Full-length PB1-F2, Nter, and pCter were not soluble at physiological pH. PB1-F2 is a positively charged protein, as are its N- and C-terminal domains (theoretical pI 10.21, 8.1, and 11.85, respectively). This suggests that basic and neutral pH values may favor protein self-associations, whereas acid pH will decrease electrostatic attractions between molecules and impede protein aggregations. To verify this, we applied DLS measurements to determine protein hydrodynamic diameters (R_H) in buffer solutions of pH ranging from pH 3 to 10 (Fig. 1*A*). The sizes obtained from DLS measurements are usually higher than real because protein particles in solution are dynamic, non-spherical, and solvated. Usually, small monomeric proteins (molecular mass ~10 kDa) have the R_H between 1 and 10 nm. At pH 3, full-length PB1-F2, Nter, and pCter had R_H of 4.5, 2.5, and 6 nm, respectively (Fig. 1*A*). This suggests that all three proteins were monomeric. Full-length PB1-F2 and Nter remained monomeric at acidic pH < 6, but strongly aggregated at neutral and basic pH values (R_H of several hundred nanometers). In contrast, pCter aggregated from pH 4 to 10 and, thus, was only found soluble at pH 3 (Fig. 1*A*).

Because PB1-F2 was reported to adopt different conformations, the secondary structure of the proteins at various pH values was investigated by far-UV CD (Fig. 1*B*). At pH 5, the

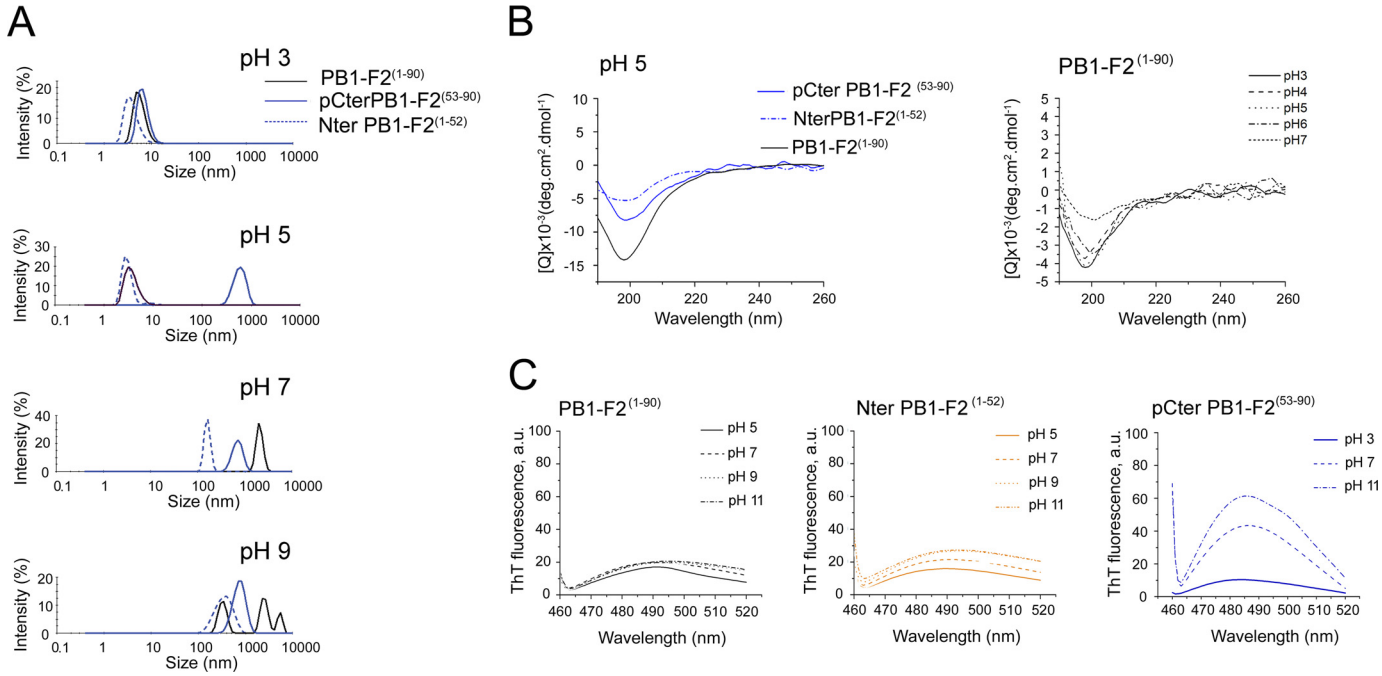

FIGURE 1. **pH-dependent structural transition of PB1-F2.** *A,* dynamic light scattering of full-length, N-terminal, and C-terminal domains of PB1-F2 over a pH range from 3 to 9 recorded at 20 °C. *B,* CD spectra of PB1-F2 proteins at pH 5 (*left panel*). Conformational transition of full-length PB1-F2 measured by CD spectroscopy upon pH variation (*right panel*). The concentration of proteins was 20 μM. *C,* ThT fluorescence was recorded in the PB1-F2 protein solution at various pH values. No chemical or thermal treatments were performed on proteins. *a.u.,* absorbance units. Experiments were performed in 100 mM sodium acetate buffer (pH 3–7) and 100 mM phosphate buffer (pH 8–11) at 20 °C.

full-length PB1-F2 exhibited the canonical features of the random coiled structure with a minimum at 198 nm (Fig. 1*B*). This finding confirms that monomeric PB1-F2 is a disordered protein in aqueous solutions as we previously reported (27). Similarly to the full-length PB1-F2, both Nter and pCter had no secondary structure at acidic pH, as presented in Fig. 1*B* (*left panel*). At pH ≥ 6, CD spectra of full-length PB1-F2 showed a small red shift in the far-UV signal minimum and a decrease in minimum intensity (Fig. 1*B*, *right panel*). The red shift in PB1-F2 ellipticity was a function of pH and, thus, probably rose from the conformational switch between two populations predominant at acidic and basic pH, respectively.

To determine whether aggregated PB1-F2 was assembled in amyloid-like structures, protein solutions were stained with ThT. ThT is a fluorescent dye that recognizes diverse types of amyloids because it binds to their commune morphological motif rich in regular cross-β-sheets (30). Fig. 1*C* shows that full-length PB1-F2 and Nter weakly bound ThT, over the pH range studied, suggesting the absence of cross-β-sheet structure. In contrast, ThT fluorescent intensity increased up to 10-fold for pCter at pH ≥ 7 (Fig. 1*C*), strongly suggesting that the C-terminal domain of PB1-F2 spontaneously fold into amyloid-like structures in neutral and basic aqueous solutions.

Membrane Permeabilization—Molecular dynamic stimulations and electrophysiological measurements suggested that PB1-F2, and notably its C-terminal domain, is able to form nonselective pores within membrane bilayers (18). To check this, we incubated full-length PB1-F2, Nter, or pCter with LUV containing a fluorescent probe calcein. The amount of calcein leakage upon protein additions was measured to quantify the relative alteration of membrane integrity. Regarding the positive net charge of proteins we prepared negatively charged LUV composed of PC/PS (1:1 molar ratio) and incubated them with proteins at various concentrations. As expected, full-length PB1-F2 and pCter destabilized negatively charged LUVs and released efficiently entrapped calcein (Fig. 2*A*). The addition of only 100 nM pCter yielded to a complete calcein leakage. In contrast, 1 μM Nter induced minimal membrane damage (<10%), whereas 1 μM full-length PB1-F2 permeabilized up to 60% of liposomes (Fig. 2*A*). These findings are in a row with the proposed mechanism that the C-terminal domain of PB1-F2 destabilizes the lipid bilayer. When proteins were added to neutral PC lipid vesicles only a small dye release was observed (< 20%) (Fig. 2*B*). This indicates that PB1-F2-membrane interactions are electrostatically driven, and that the membrane lipid composition determines the PB1-F2 capacity to destabilize lipid bilayer.

To further verify whether lipid negative charge is needed for PB1-F2-membrane interaction, PB1-F2 was incubated with either neutral PC LUVs or negatively charged PS/PS LUVs (1:1 molar ratio) in sodium acetate buffer (pH 5), and subsequently ultracentrifuged to separate lipids from the soluble fraction. Fractions were then subjected to SDS-PAGE analysis and proteins were visualized by Coomassie Blue staining. Full-length PB1-F2 was associated exclusively with negatively charged PC/PS vesicles, whereas it was equally distributed in aqueous and lipid fractions of the zwitterionic PC vesicles (Fig. 2*C*). It appears, thus, that PB1-F2 membrane binding correlates with membrane leakage. Both processes seem to be electrostatically driven.

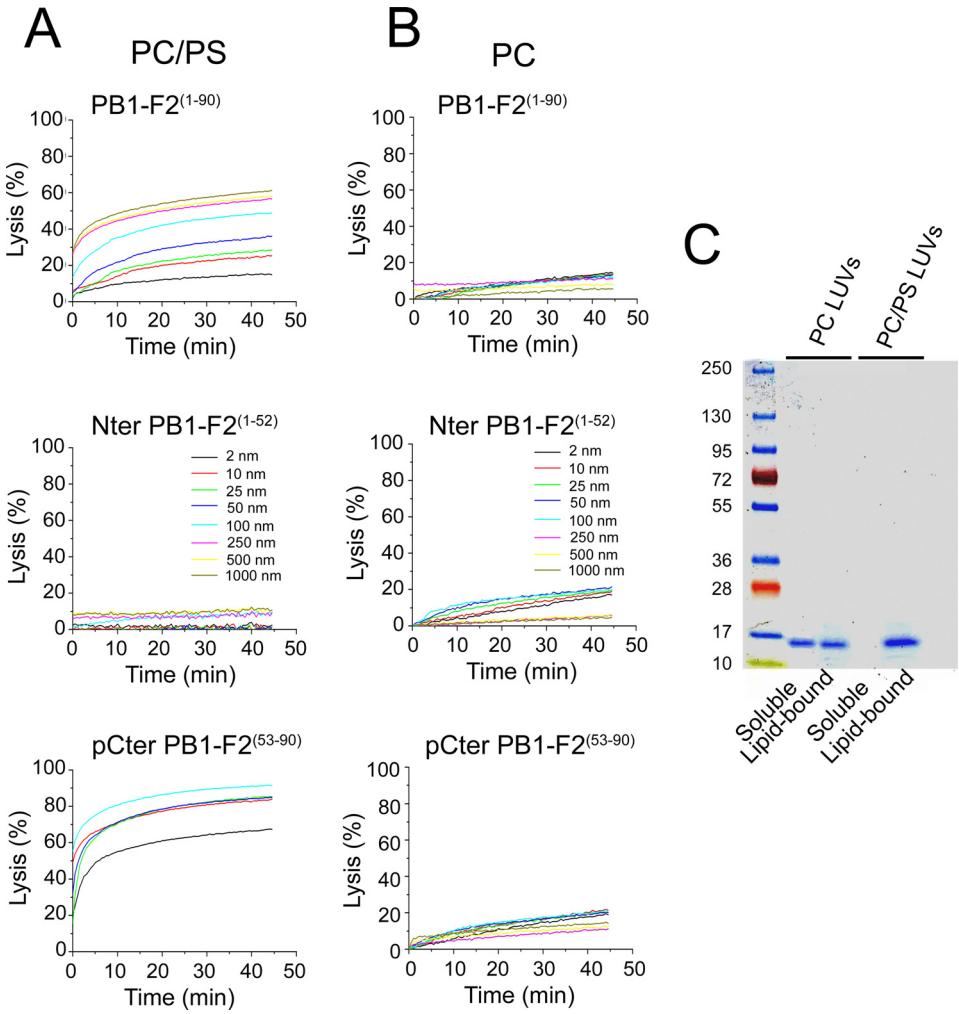

FIGURE 2. **Membrane permeabilization by PB1-F2.** Liposomes of various lipid compositions were assayed for calcein release upon addition of PB1-F2 in the concentration range from 2 nM to 1 μM. Measurements were done in 10 mM sodium acetate buffer (pH 5) at room temperature. *A,* full-length PB1-F2 and pCter but not Nter permeabilize anionic liposomes. *B,* PB1-F2 peptides do not destabilize liposomes of neutral net charge. *C,* full-length PB1-F2 was incubated with anionic or neutral liposomes. Membrane-associated (lipid-bound) protein molecules were separated from free protein molecules (soluble) by ultracentrifugation. Note that PB1-F2 preferentially binds to the phospholipidic liposomes of negative net charge.

Secondary Structure of PB1-F2 in a Membrane Environment—To test whether amyloid structures were formed by PB1-F2 incubated with anionic PC/PS LUVs (1:1 molar ratio) the protein-liposome preparations were stained with ThT. All three preparations strongly bound ThT and gave the increase in ThT fluorescence emission up to 10-fold compared with that of LUVs alone (Fig. 3*A*). The same experiments were performed with neutral LUVs made of PC but no increase in ThT fluorescence was observed with any of three proteins (data not shown). The results indicate that the negative net lipid charge is necessary to favor amyloid aggregation of PB1-F2 upon membrane binding.

To verify whether PB1-F2 binding to negatively charged lipids alters membrane integrity, we used negative staining to visualize liposomes incubated with the full-length PB1-F2. Before addition of PB1-F2, the liposomes were of spherical appearance with diameters ranging from 80 to 400 nm (Fig. 3*B*). Liposomes incubated with PB1-F2 were less numbered and were mostly fragmented into smaller vesicles illustrating the destabilizing effect of PB1-F2 on membrane integrity. In addition, electron microscopy confirmed that PB1-F2 was assembled into fibers upon binding to membranes. Two types of PB1-F2 aggregates can be observed in Fig. 3*B*: small spherical particles with an average diameter of 20–100 nm (*red arrows*) corresponding to PB1-F2 oligomers, and mature amyloid fibers of several hundred nanometer length (*red asterisks*).

PB1-F2 Cytotoxicity—An important question to raise concerning the interaction between PB1-F2 and membranes is whether PB1-F2 can destabilize the cellular membrane and induce a cytotoxic effect. Indeed, many cationic peptides have hemolytic activity on both prokaryotic and eukaryotic cells through direct membrane disruption (31, 32). To avoid indirect cytotoxicity of an acid pH, all cytotoxic tests were performed at physiological pH 7.4, *i.e.* the condition when PB1-F2 cannot be solubilized. At pH 7.4, both full-length PB1-F2 and pCter aggregate, but adopt different conformational states: full-length PB1-F2 forms amorphous aggregates (ThT negative), whereas its C terminus forms amyloid-like structures (ThT positive). The AFM observation of proteins in PBS (pH 7.4), confirmed these features: pCter mainly formed spherical oligomers and some fragmented fibrils, whereas full-length PB1-F2 was found to adopt shapeless aggregate structures (Fig. 4, *A* and *B*).

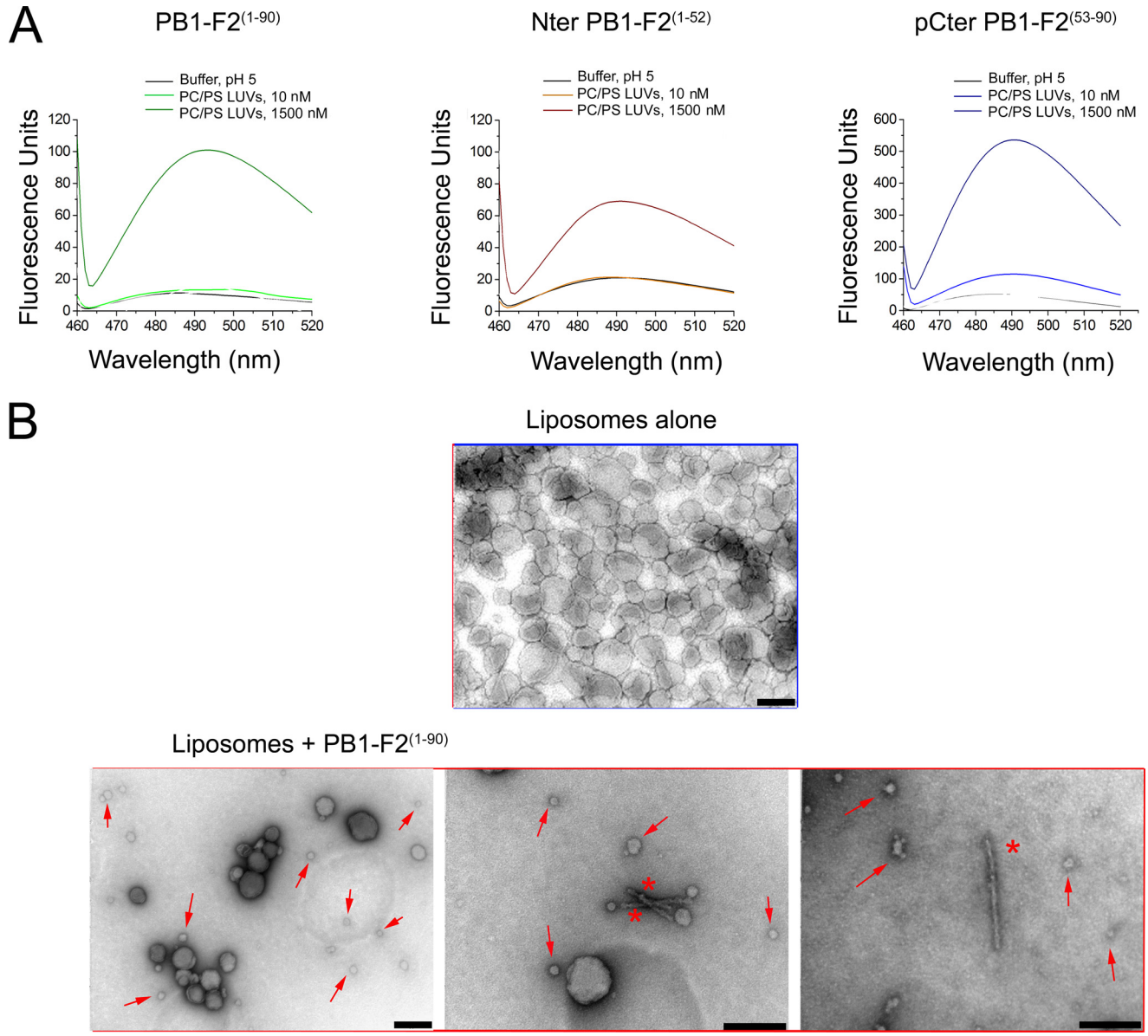

FIGURE 3. **Both PB1-F2 and lipid vesicles undergo structural alternations upon interacting.** *A,* ThT emission fluorescent spectra of full-length, N- and C-terminal domains of PB1-F2 (100 μM) were incubated with anionic LUVs (total lipids, 0.5 mg/ml). Note that all three PB1-F2 peptides form amyloid-like structures when admixed to a negatively charged liposome solution of pH 5. *B,* electron microscopy of negatively stained extruded anionic liposomes (1 mg/ml, total lipids) incubated with full-length PB1-F2 (20 μM) in 10 mM sodium acetate buffer (pH 5). *Red asterisks* point to long fibrillary structures, and *red arrows* point to small spherical structures probably corresponding to protein oligomers. *Bars*, 200 nm.

To test whether PB1-F2 has an antimicrobial effect two different bacterial strains *B. subtilis* and *E. coli* were incubated with various concentrations of full-length PB1-F2 or pCter in LB medium (Fig. 4*C*). *B. subtilis* are Gram-positive bacteria possessing a single unit lipid membrane, whereas the Gram-negative bacteria *E. coli* have inner and outer cell membranes. When *E. coli* was incubated with either full-length PB1-F2 or pCter (0.5–20 μM, monomer equivalent concentration), no decrease in optical density was detected at 600 nm upon 24 h monitoring compared with the control (Fig. 4*C*, *left panel*). The normal proliferation of Gram-negative bacteria suggests that PB1-F2 has no direct antibacterial activity. However, 20 μM oligomeric pCter significantly reduced kinetics of *B. subtilis* growth within the first few hours of incubation, as shown in Fig. 4*C* (*right panel*). The same concentration of aggregated full-length PB1-F2 had no antibacterial effect on *B. subtilis* (Fig. 4*C*).

To test whether PB1-F2 is cytotoxic toward a mammalian cell, PB1-F2 effects on alveolar epithelial cells (A549) were analyzed using the MTT assay. In this assay, cellular reduction of the tetrazolium dye MTT was an indicator of cell viability (33). Addition of amorphous aggregates of the full-length PB1-F2 showed no significant MTT reduction (Fig. 5*A*). In contrast, addition of oligomerized pCter to the cell medium resulted in a marked decrease in MTT reduction in A549 cells (Fig. 5*B*). The decrease is statistically highly significant with respect to controls performed with A549 cells incubated with PBS. Observed toxicity depended on the pCter concentration: the inhibition of MTT reduction ranged from 10 ± 5% (for 1 μM pCter PB1-F2(53–90)) to 50 ± 10% (for 20 μM pCter PB1-F2(53–90)) with

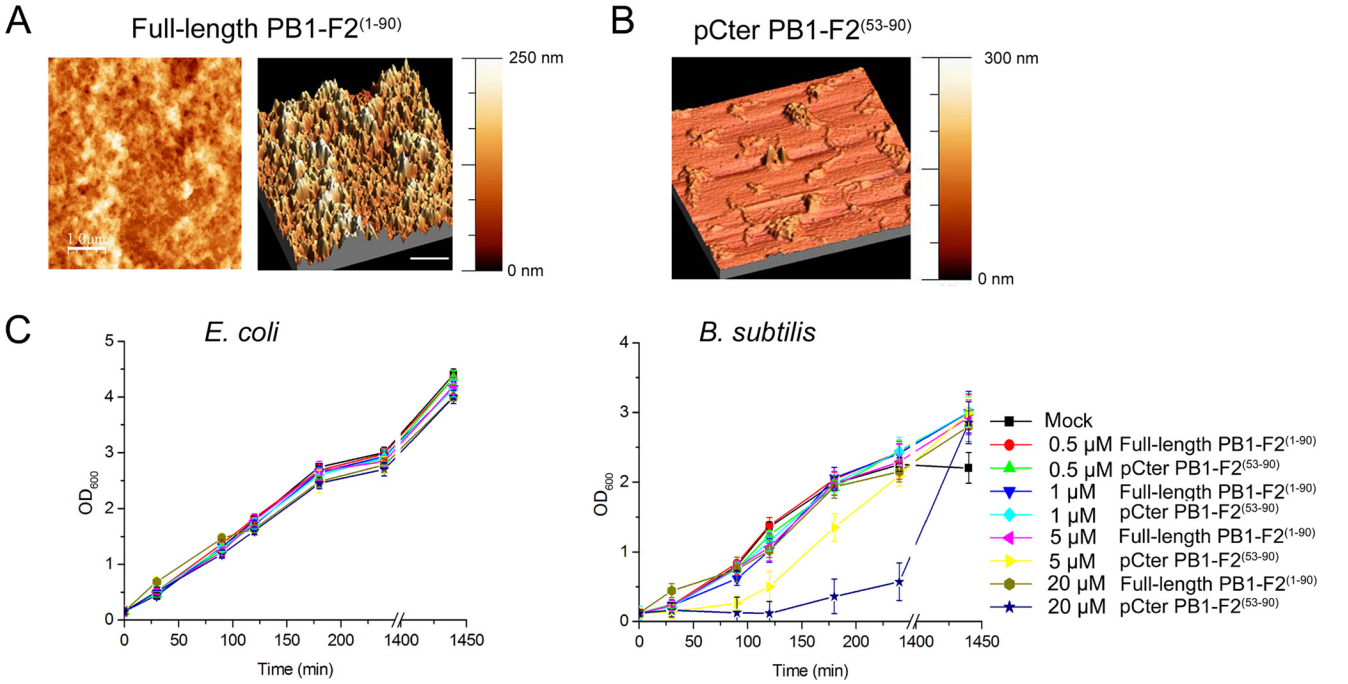

FIGURE 4. **Antimicrobial activity of full-length and C-terminal domain of PB1-F2 at pH 7.4**. *A,* AFM images showing unstructured aggregates formed by full-length PB1-F2 in PBS (pH 7.4). *Bar*, 1 μm. *B,* AFM image of the C-terminal domain of PB1-F2 shows protein oligomers and fibers. *Bar*, 1 μm. *C*, the optical density recorded at 600 nm for *E. coli* and *B. subtilis* cultures at different time intervals. Bacterial cultures were diluted to start at A_{600} of 0.1 and then grown in the presence of 0.5–20 μM PB1-F2(1–90) aggregates, 0.5–20 μM pCter oligomers, or LB media alone (mock). pCter oligomers showed a concentration-dependent reduction in *B. subtilis* cell growth during the first few hours. In contrast, PB1-F2 aggregates and mock failed to reduce bacteria growth. Note that no inhibition of *E. coli* growth was observed upon their incubation with either full-length or the C-terminal domain of PB1-F2. *Error bars* indicate the standard error in triplicate experiments.

respect to the control experiments. The optical microscopy observation of the A549 cells treated with pCter oligomers showed drastic changes in cell morphology, as illustrated in Fig. 5*C*. In contrast, no effect was observed on cell morphology and density after cell incubations with the equivalent concentrations of amorphous PB1-F2 (Fig. 5*C*). These results point out that cytotoxicity of PB1-F2 depends on the protein quaternary structure.

To verify this hypothesis we tested whether cytotoxicity can be induced by the full-length PB1-F2 pre-polymerized into amyloid fibrils. For this PB1-F2 was incubated with 0.005% (w/v) SDS in PBS (pH 7.4) (Fig. 6, *A* and *B*). We previously showed that PB1-F2 converts into amyloid-like structures in the presence of a diluted anionic detergent SDS (concentration of SDS below its CMC of 0.23% (w/v)) (27, 29, 34). The long PB1-F2 fibrils obtained were of micron sizes and showed no significant cytotoxic effect on A549 cells (Fig. 6*C*). However, when PB1-F2 fibrils were fragmented by sonication to nanoscale particles (Fig. 6*B*) and added to the cell culture medium, a pronounced decrease in MTT reduction levels was observed (Fig. 6*C*). Remarkably, the cytotoxic effect observed with fragmented PB1-F2 fibrils were similar to those observed with oligomerized pCter in Fig. 5*B*. The obtained data confirm that cytotoxicity mediated by PB1-F2 is caused by the protein amyloid-like oligomers.

To test whether oligomerized Nter can also reduce cell viability, we tried to pre-fibrilize Nter with 0.005% (w/v) SDS in PBS (pH 7.4). However, incubation of Nter with SDS at physiological pH did not yield amyloid fibril formation within the experimental time scale (Fig. 6, *D* and *E*). Instead, Nter particles had $R_H < 10$ nm and weekly bound ThT. These Nter particles cannot be fragmented by sonication (Fig. 6*E*) and fail to reduce MTT in A549 cells (Fig. 6*F*). Thus, it appears that only nanoscaled amyloids of PB1-F2 can damage epithelial cells.

Finally we verified whether membrane disruption was a factor in the virulence associated with PB1-F2. For this, U937 and A549 cells were infected with wild-type A/WSN/1933 (H1N1) or the PB1-F2 knocked out mutant virus (ΔF2). It was previously shown that there is no significant difference in progeny virus titers between wild-type and ΔF2 viruses upon infection of various cell lines and tissues (22, 35). In addition, it was shown that PB1-F2 expression starts at early stages of the viral cycle, when it is barely detectable in its monomeric form (22, 27, 34). At the later stage of infection the monomeric PB1-F2 is almost undetectable because the protein accumulates as amyloid-like oligomers as has been demonstrated in both A549 and U937 IAV-infected cells (22, 27, 34).

Here, to quantify the membrane damages, infected cells were harvested and analyzed for acridine orange fluorescence by flow cytometry. Acridine orange easily traverses the cell membrane and accumulates in lysosomes. During necrosis, which is characterized by the loss of membrane function and its structural integrity, lysosomes are ruptured and red fluorescence of the dye decreases (36). As shown in Fig. 7 there was no significant difference in acridine orange staining between cells infected with wild-type and mutant virus at 8 h post-infection. In contrast, wild-type virus had a much stronger ability to decrease acridine orange red fluorescent staining than mutant ΔF2 virus at 24 h post-infection. This suggests that PB1-F2 induce membrane disruption of

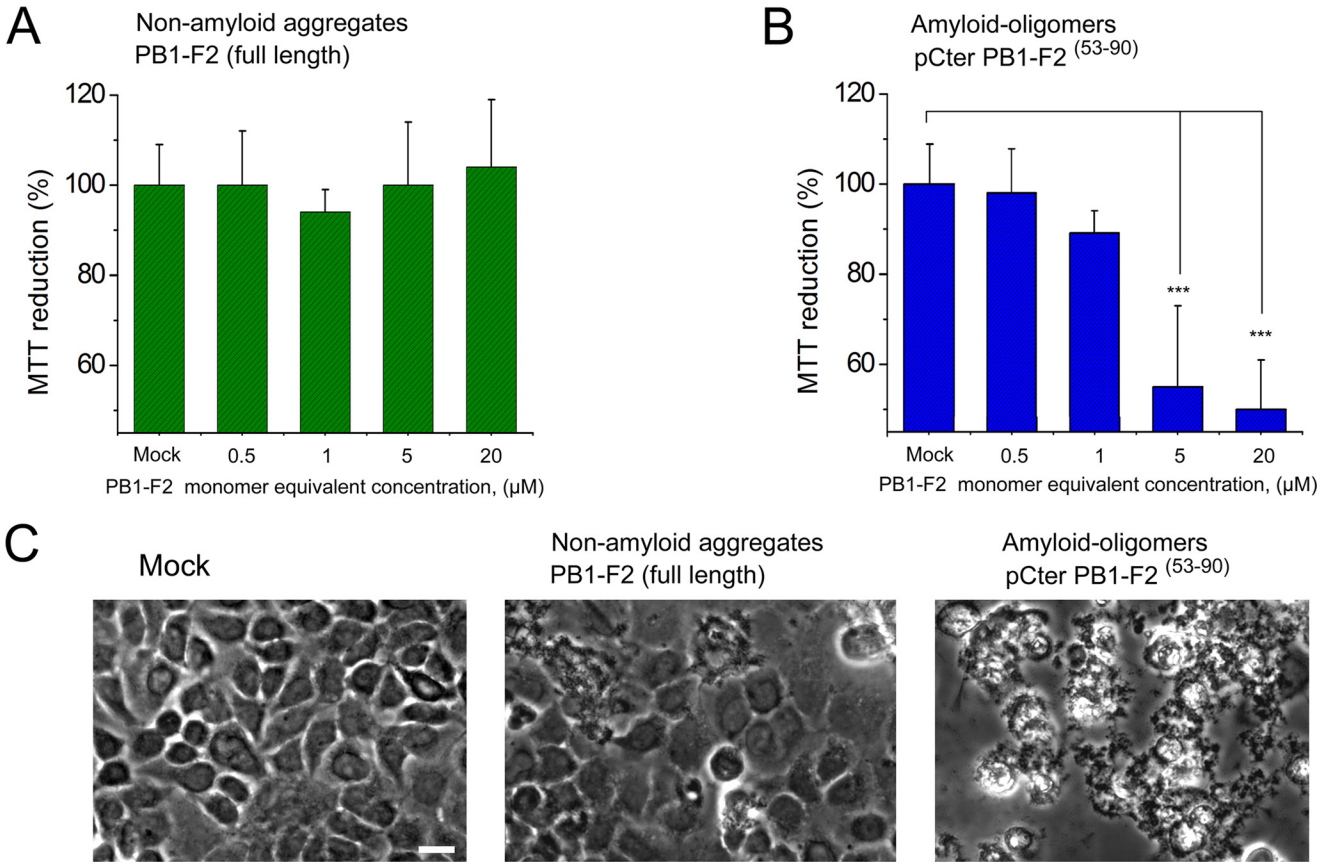

FIGURE 5. **PB1-F2 oligomers are cytotoxic.** *A,* MTT reduction in cells incubated with full-length PB1-F2 amorphous aggregates. *B,* MTT reduction in cells incubated with the C terminus amyloid-like oligomers in PBS buffer. The reduction of MTT was assayed after A549 cell incubation with PB1-F2 for 24 h. The % of MTT reduction relative to that of control cells incubated with PBS is plotted. The *error bars* represent S.D. of the means over the 10 replicates, *, correspond to p value < 0.05; **, $p < 0.01$; and ***, $p < 0.001$. *C,* cells incubated with full-length PB1-F2, pCter, or PBS buffer for 24 h were observed by optical microscopy to visualize their morphology. *Bar,* 10 μm

infected cells only at later stages of the viral cycle. In consequence it appears that the PB1-F2 membrane disruption in IAV-infected cells is associated with PB1-F2 assembled into amyloid structures.

To further check the impact of oligomerized PB1-F2 on cell membrane integrity upon infection, U937 cells were infected with wild-type and ΔF2 viruses and observed using electron microscopy at 24 h post-infection. Morphological modifications of the plasma membrane in influenza virus-infected monocytes are largely unknown and clearly need to be addressed in detail. Nevertheless, plasma membranes of wild-type virus-infected cells seem to release membrane vesicles and show more important lipid bilayer fragmentation and membrane damages than ΔF2-infected cells or mock-infected cells (Fig. 8). Hence, at late stages of infection, membrane structure integrity of wild-type virus-infected cells was destabilized, whereas plasma membranes of ΔF2-infected cells appeared to be more preserved. Altogether, our results show that lytic activity of PB1-F2 assembled into amyloid structures contributes to cell membrane damage upon infection.

Discussion

Accessory IAV protein PB1-F2 contributes to virulence by a still poorly understood mechanism that seems to be complex and host- and strain-specific (12, 37). Here we demonstrated that the PB1-F2 interaction with membranes depends on charge and composition of the lipid bilayer, and that PB1-F2 cytotoxicity depends on its supramolecular structure.

When expressed within infected cells, PB1-F2 has intimate relationships with cellular components that are facilitated by its structural flexibility. PB1-F2 interaction with membranes has previously been suggested because the synthetic PB1-F2 protein was shown to permeabilize mitochondrial membrane leading to its destabilization, depolarization, and apoptosis (17, 18). We present several lines of evidence that PB1-F2 undergoes conformational conversion upon binding negatively charged phospholipid membrane and assembles into amyloid-like structures. The protein conversion was not observed with a neutral lipid bilayer. Interestingly, the N-terminal domain of PB1-F2 oligomerizes to amyloids in the membrane mimic environment in sodium acetate buffer (pH 5), but not in PBS (pH 7.4). This suggests that low ionic strength and a mild acidification of the Nter molecule are needed to allow its polymerization to amyloid structures. Furthermore, Nter failed to induce cytotoxic effects on epithelial cells in cell medium of physiological pH. Currently many low pathogenic AIV strains do not express full-length PB1-F2 or express its C terminally truncated PB1-F2 form (PB1-F2

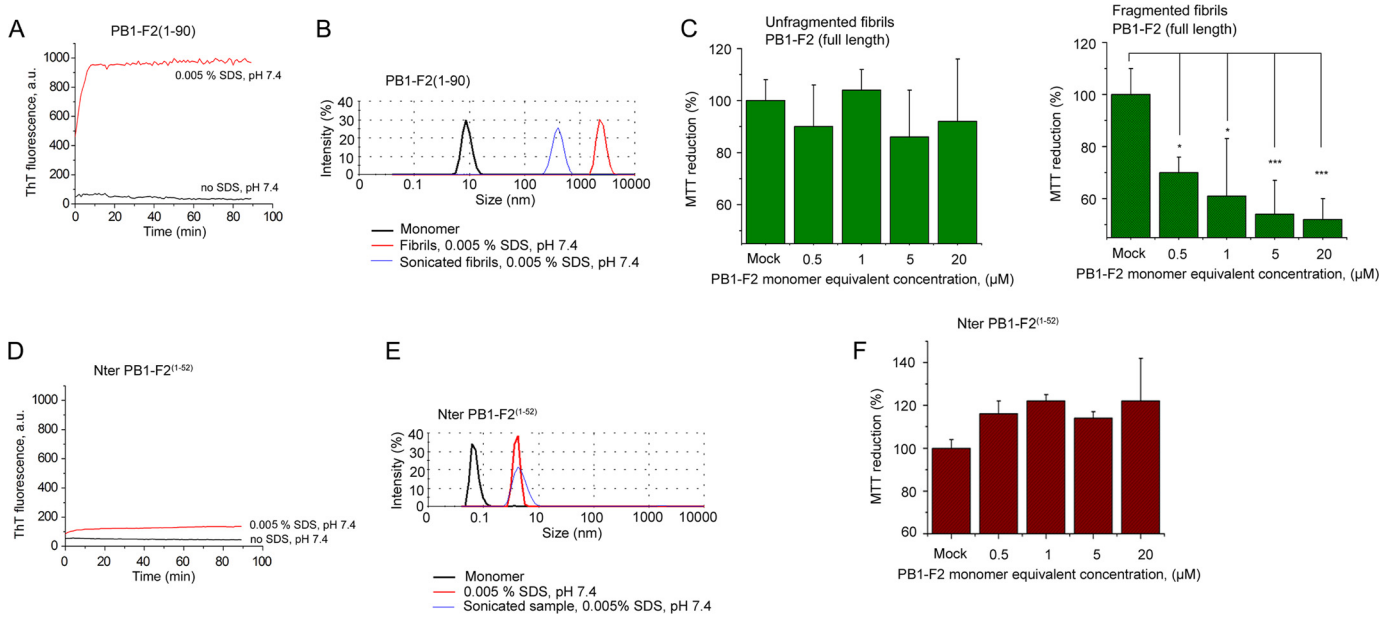

FIGURE 6. **PB-F2 fragmented amyloid fibers are cytotoxic.** *A,* polymerization of full-length PB1-F2 was obtained in PBS buffer solution (pH 7.4), containing 0.005% (w/v) SDS. ThT binding to the fibers formed was recorded at 498 nm upon the excitation wavelength 445 nm. Note that no amyloid-like structures were formed without SDS. *B,* DLS analysis of the full-length PB1-F2 at pH 5 (monomers) and the SDS/PBS solution (pH 7.4) (fibrils). Fibrils were fragmented by 20 min sonication (sonicated fibrils). *C,* MTT reduction in A549 cells incubated with full-length PB1-F2 pre-polymerized to amyloid fibrils of several micrometer sizes (*left panel*) and MTT reduction in A549 cells incubated with PB1-F2 fragmented fibrils of nanoscale sizes. *D,* polymerization of the N-terminal domain of PB1-F2 was monitored in PBS buffer solution (pH 7.4) containing 0.005% (w/v) SDS. No significant ThT signal increase was observed. ThT emission intensity was recorded at 498 nm upon excitation at 445 nm. *E,* DLS analysis of Nter at pH 5 (monomers) and SDS/PBS solution (pH 7.4) (small agregates). *F,* MTT reduction in A549 cells incubated with Nter pre-aggregated in SDS/PBS solution. Note that no significant reduction in MTT was observed with Nter. The reduction of MTT was assayed after the cells were incubated with various PB1-F2 for 24 h. The % of MTT reduction relative to that of control cells incubated with PBS is plotted. The *error bars* represent mean ± S.D. over the total of 10 replicates, *, correspond to p value < 0.05; **, $p < 0.01$; and ***, $p < 0.001$.

(1–52)) (12, 38). Virus expression of truncated PB1-F2, which fails to induce cytotoxicity under physiological conditions, may be correlated to the viral fitness to prevent the deleterious cytotoxicity of the full-length PB1-F2.

Our structural characterizations demonstrate that recombinant PB1-F2 is monomeric only in solutions of acidic pH. CD spectra analysis indicates that monomeric full-length PB1-F2, Nter, and pCter are inherently disordered proteins. The increase of pH caused aggregation and precipitation of PB1-F2. Interestingly, the C-terminal domain of PB1-F2 converts to amyloid-like oligomers at neutral and basic pH values without any treatment. This spontaneous conformational switch additionally points out that the C-terminal part of PB1-F2 is initially deprived of any secondary structure at these pH values. Indeed, whereas most α-helical proteins such as β_2-microglobulin, lysozyme, or prion protein need some chemical or thermal treatment to convert into amyloid structures *in vitro* (39–41), natively disordered proteins as Aβ, Shadoo, α-synuclain may switch to amyloid-like forms without recourse to denaturation treatment (42–45).

Although PB1-F2 was proposed to self-organize into a membrane non-selective pore upon interacting with membranes (18), other mechanisms leading to membrane permeabilization cannot be excluded. For instance, it was shown that Shadoo, α-synuclein, and the type 2 diabetes-associated islet amyloid polypeptide extensively damage the membrane when they start to aggregate because their growing entities capture and extract lipids from the bilayer (44, 46–48). One amyloid protein may, also, employ different mechanisms to interact with membranes depending on the membrane lipid composition (49). For instance, oligomerized prion was shown to disturb anionic phospholipid membrane through a detergent model in which the membrane leakage is caused by the removal of lipid-prion micelles. In contrast, prion oligomer accumulation on the cholesterol containing zwitterionic liposomes was shown to induce a loss of raft domains, which destroys membrane integrity (49). The physical basis for PB1-F2 membrane disruption remains to be elucidated, but our results suggest PB1-F2 lysis activity is related to the protein oligomers.

Our results demonstrated that cytotoxicity of PB1-F2 depends on the protein conformational state and its supramolecular organization. Monomeric PB1-F2 added to a solution of physiological pH aggregates to amorphous structures and shows no cytotoxicity toward epithelial cells. However, PB1-F2 amyloid-like oligomers or fragmented nanoscaled fibers are highly cytotoxic. At later stages of an IAV infection PB1-F2 cannot be detected as monomeric within infected cells (≥8 h.p.i.) but assembled into amyloid oligomers and fibers (22, 27, 34). In consequence, in the final step of the lytic cycle of influenza virus, PB1-F2 released in extracellular medium is probably assembled into amyloid structures. Similarly, we observed the membrane disruption in IAV-infected cells only at later stages of the viral cycle. Amyloid oligomers formed by different proteins are reported to share similar cytotoxicity regardless of the protein sequence probably due to their unique physical and morphological properties (50–52). Moreover, the interaction between amyloid proteins and cell membranes is thought to play an important role in amyloid pathologies. Our results sug-

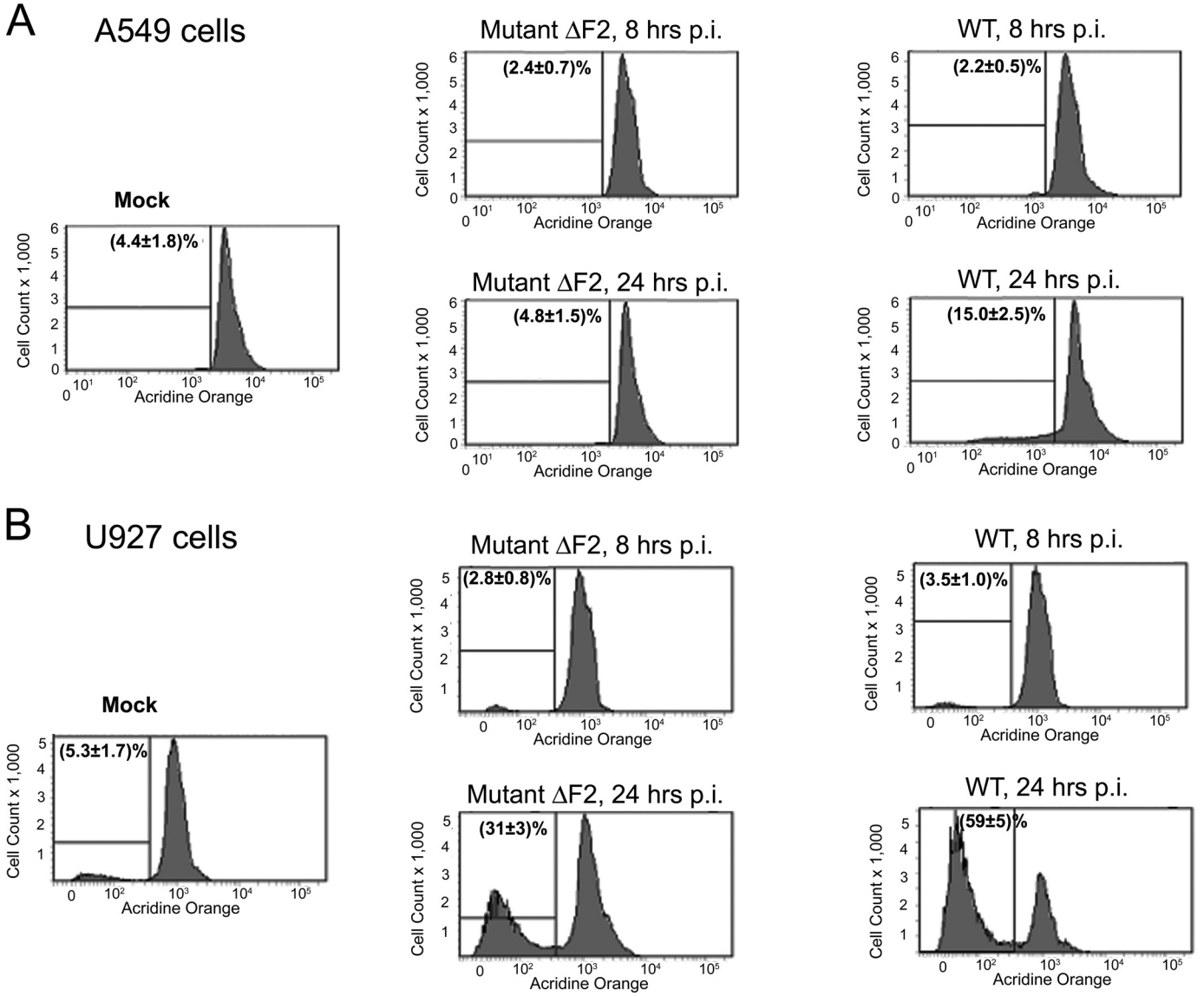

FIGURE 7. **PB-F2 oligomers in infected cells increases cell death at a later stage of infection.** Viability of human alveolar epithelial A549 cells (*A*), and human monocyte U937 cells (*B*), infected with wild-type or mutant ΔF2 virus, was estimated by acridine orange staining and flow cytometry analysis. *Numbers* in each highlighted quadrant reflect the percentage of cells in the necrotic zone. Data are the means of at least three separate experiments. Note that there was a significant difference in acridine orange fluorescence between cells infected with wild-type and mutant IAV at 24 h but not at 8 h postinfection. This suggests that oligomerized but not monomeric PB1-F2 destabilize membrane structure integrity in IAV-infected cells.

gest that immunopathological disorders observed during IAV infections may originate from the PB1-F2 amyloid oligomers interaction with cell membranes.

It is interesting to note that previous investigations of PB1-F2 from the extracellular matrix has shown that only PB1-F2 aggregated in particles >100 kDa can trigger an inflammatory response in macrophages (53). Moreover, PB1-F2 targeting mitochondria was also reported to be assembled into highly ordered oligomers (15). These studies are in accordance with our finding that oligomerized PB1-F2, but not monomeric, is a factor of virulence.

A significant proportion of severe influenza virus illnesses are associated with influenza virus-bacterium superinfections. Similarly, infection of mice with IAV expressing PB1-F2 was reported to significantly enhance the predisposition to secondary bacterial infections (25, 26). We observed no effect of PB1-F2, either amorphous or amyloidal, on *E. coli* growth and only an ephemeral inhibitory effect on *B. subtilis* growth. It appears, thus, that the PB1-F2-mediated increase in secondary bacterial infections during IAV infection does not rise from the direct interaction PB1-F2 bacteria but rather from the impairment of host immune cells by PB1-F2.

In conclusion, PB1-F2 cytotoxicity and membrane lysis activity are correlated with the protein assembling into amyloid structures. PB1-F2 is an intrinsically disordered protein, which shows high structural flexibility allowing it to easily adopt the amyloid form in an anionic hydrophobic environment. The high cytotoxicity of PB1-F2 amyloids observed suggests that an impediment of the protein assembling into amyloid oligomers might prove useful in treatment of several forms of influenza infections. Future studies should determine if some host proteins may be involved in modulating PB1-F2 molecular organi-

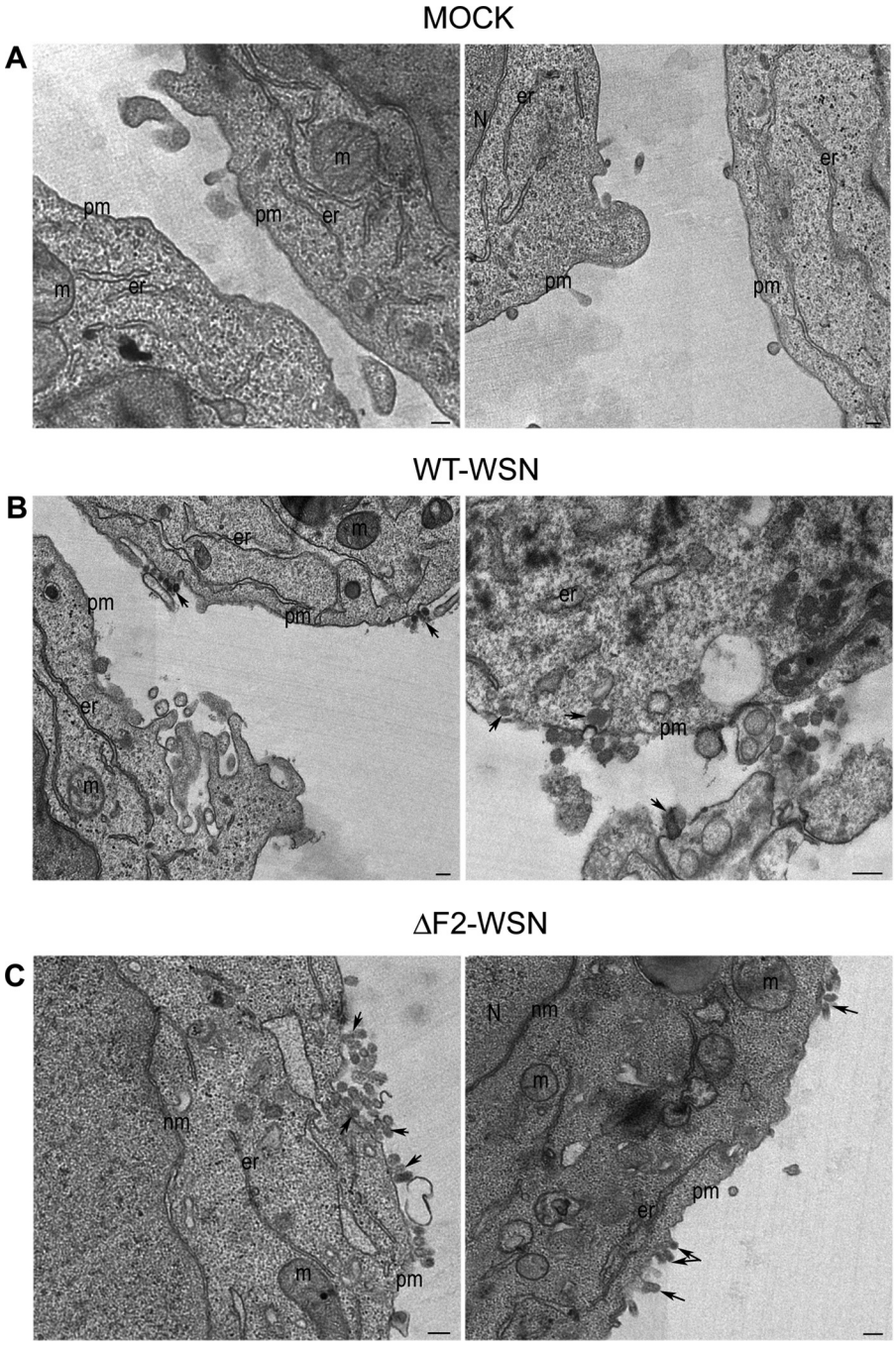

FIGURE 8. **Visualization of IAV-infected U937 cells at late stages of infection by electron microscopy.** Representative thin section electron micrographs showing: *A,* uninfected cells; *B,* cells infected with wild-type WSN virus; and *C,* cells infected with mutant ΔF2 virus. Note that plasma membranes of uninfected and cells infected with ΔF2 virus are continuous double layers, whereas membranes of cells infected with wild-type virus are rather thinner and discontinuous, with many membrane vesicles in the vicinity to virus budding. *Arrows* point to viral particles. *er*, endoplasmic reticulum; *m*, mitochondria; *pm*, plasmic membrane; *N*, nucleus; *nm*, nuclear membrane. *Scale bars*, 200 nm.

zation, and provide additional tools to prevent the contribution of PB1-F2 to the pathophysiology of infection.

Author Contributions—J. V. conceived the study, performed experiments, and wrote the paper. C. A. R. and C. C. purified proteins, C. C. performed experiments in Figs. 3*C* and 5*C*, provided cells and viruses. S. M. performed AFM measurements. C. P. performed electron microscopy. B. D. C. and N. B. provided assistance for experiments in Fig. 7. All authors provided critical feedback on the manuscript and approved the final version of the manuscript.

Acknowledgments—We acknowledge Dr Sandrine Auger (INRA, Jouy en Josas) for the support of B. subtilis, Dr. Mohammed Moudjou (INRA, Jouy en Josas) for protein purification, and Dr. Stephane Biacchesi (INRA, Jouy en Josas) and Dr. Aurore Vidy (Insitut Pasteur, Paris) for valuable discussions. This work has benefited from the facilities and expertise of protein purification (VIM, INRA) and electron microscopy MIMA2 MET (GABI, INRA) platforms, Jouy en Josas, France.

References

1. Wright, P. F., Neumann, G., and Kawaoka, Y. (2007) *Orthomyxoviruses*, Lippincott Williams & Wilkins, Philadelphia, PA
2. Jagger, B. W., Wise, H. M., Kash, J. C., Walters, K. A., Wills, N. M., Xiao, Y. L., Dunfee, R. L., Schwartzman, L. M., Ozinsky, A., Bell, G. L., Dalton, R. M., Lo, A., Efstathiou, S., Atkins, J. F., Firth, A. E., Taubenberger, J. K., and Digard, P. (2012) An overlapping protein-coding region in influenza A virus segment 3 modulates the host response. *Science* **337,** 199–204
3. Muramoto, Y., Noda, T., Kawakami, E., Akkina, R., and Kawaoka, Y. (2013) Identification of novel influenza A virus proteins translated from PA mRNA. *J. Virol.* **87,** 2455–2462
4. Vasin, A. V., Temkina, O. A., Egorov, V. V., Klotchenko, S. A., Plotnikova, M. A., and Kiselev, O. I. (2014) Molecular mechanisms enhancing the proteome of influenza A viruses: an overview of recently discovered proteins. *Virus Res.* **185,** 53–63
5. Wise, H. M., Foeglein, A., Sun, J., Dalton, R. M., Patel, S., Howard, W., Anderson, E. C., Barclay, W. S., and Digard, P. (2009) A complicated message: identification of a novel PB1-related protein translated from influenza A virus segment 2 mRNA. *J. Virol.* **83,** 8021–8031
6. Wise, H. M., Hutchinson, E. C., Jagger, B. W., Stuart, A. D., Kang, Z. H., Robb, N., Schwartzman, L. M., Kash, J. C., Fodor, E., Firth, A. E., Gog, J. R., Taubenberger, J. K., and Digard, P. (2012) Identification of a novel splice variant form of the influenza A virus M2 ion channel with an antigenically distinct ectodomain. *PLoS Pathog.* **8,** e1002998
7. Chen, W., Calvo, P. A., Malide, D., Gibbs, J., Schubert, U., Bacik, I., Basta, S., O'Neill, R., Schickli, J., Palese, P., Henklein, P., Bennink, J. R., and Yewdell, J. W. (2001) A novel influenza A virus mitochondrial protein that induces cell death. *Nat. Med.* **7,** 1306–1312
8. Krumbholz, A., Philipps, A., Oehring, H., Schwarzer, K., Eitner, A., Wutzler, P., and Zell, R. (2011) Current knowledge on PB1-F2 of influenza A viruses. *Med. Microbiol. Immunol.* **200,** 69–75
9. Kash, J. C., Tumpey, T. M., Proll, S. C., Carter, V., Perwitasari, O., Thomas, M. J., Basler, C. F., Palese, P., Taubenberger, J. K., García-Sastre, A., Swayne, D. E., and Katze, M. G. (2006) Genomic analysis of increased host immune and cell death responses induced by 1918 influenza virus. *Nature* **443,** 578–581
10. La Gruta, N. L., Kedzierska, K., Stambas, J., and Doherty, P. C. (2007) A question of self-preservation: immunopathology in influenza virus infection. *Immunol. Cell Biol.* **85,** 85–92
11. McAuley, J. L., Hornung, F., Boyd, K. L., Smith, A. M., McKeon, R., Bennink, J., Yewdell, J. W., and McCullers, J. A. (2007) Expression of the 1918 influenza A virus PB1-F2 enhances the pathogenesis of viral and secondary bacterial pneumonia. *Cell Host Microbe* **2,** 240–249
12. Chakrabarti, A. K., and Pasricha, G. (2013) An insight into the PB1F2 protein and its multifunctional role in enhancing the pathogenicity of the influenza A viruses. *Virology* **440,** 97–104
13. Gibbs, J. S., Malide, D., Hornung, F., Bennink, J. R., and Yewdell, J. W. (2003) The influenza A virus PB1-F2 protein targets the inner mitochondrial membrane via a predicted basic amphipathic helix that disrupts mitochondrial function. *J. Virol.* **77,** 7214–7224
14. Yamada, H., Chounan, R., Higashi, Y., Kurihara, N., and Kido, H. (2004) Mitochondrial targeting sequence of the influenza A virus PB1-F2 protein and its function in mitochondria. *FEBS Lett.* **578,** 331–336
15. Yoshizumi, T., Ichinohe, T., Sasaki, O., Otera, H., Kawabata, S., Mihara, K., and Koshiba, T. (2014) Influenza A virus protein PB1-F2 translocates into mitochondria via Tom40 channels and impairs innate immunity. *Nat. Commun.* **5,** 4713
16. Zamarin, D., García-Sastre, A., Xiao, X., Wang, R., and Palese, P. (2005) Influenza virus PB1-F2 protein induces cell death through mitochondrial ANT3 and VDAC1. *PLoS Pathog.* **1,** e4
17. Chanturiya, A. N., Basañez, G., Schubert, U., Henklein, P., Yewdell, J. W., and Zimmerberg, J. (2004) PB1-F2, an influenza A virus-encoded proapoptotic mitochondrial protein, creates variably sized pores in planar lipid membranes. *J. Virol.* **78,** 6304–6312
18. Henkel, M., Mitzner, D., Henklein, P., Meyer-Almes, F. J., Moroni, A., Difrancesco, M. L., Henkes, L. M., Kreim, M., Kast, S. M., Schubert, U., and Thiel, G. (2010) The proapoptotic influenza A virus protein PB1-F2 forms a nonselective ion channel. *PLoS ONE* **5,** e11112
19. Mazur, I., Anhlan, D., Mitzner, D., Wixler, L., Schubert, U., and Ludwig, S. (2008) The proapoptotic influenza A virus protein PB1-F2 regulates viral polymerase activity by interaction with the PB1 protein. *Cell Microbiol.* **10,** 1140–1152
20. McAuley, J. L., Zhang, K., and McCullers, J. A. (2010) The effects of influenza A virus PB1-F2 protein on polymerase activity are strain specific and do not impact pathogenesis. *J. Virol.* **84,** 558–564
21. Conenello, G. M., Tisoncik, J. R., Rosenzweig, E., Varga, Z. T., Palese, P., and Katze, M. G. (2011) A single N66S mutation in the PB1-F2 protein of influenza A virus increases virulence by inhibiting the early interferon response *in vivo*. *J. Virol.* **85,** 652–662
22. Le Goffic, R., Bouguyon, E., Chevalier, C., Vidic, J., Da Costa, B., Leymarie, O., Bourdieu, C., Decamps, L., Dhorne-Pollet, S., and Delmas, B. (2010) Influenza A virus protein PB1-F2 exacerbates IFN-β expression of human respiratory epithelial cells. *J. Immunol.* **185,** 4812–4823
23. Varga, Z. T., Grant, A., Manicassamy, B., and Palese, P. (2012) Influenza virus protein PB1-F2 inhibits the induction of type I interferon by binding to MAVS and decreasing mitochondrial membrane potential. *J. Virol.* **86,** 8359–8366
24. Varga, Z. T., Ramos, I., Hai, R., Schmolke, M., García-Sastre, A., Fernandez-Sesma, A., and Palese, P. (2011) The influenza virus protein PB1-F2 inhibits the induction of type I interferon at the level of the MAVS adaptor protein. *PLoS Pathog.* **7,** e1002067
25. Alymova, I. V., Samarasinghe, A., Vogel, P., Green, A. M., Weinlich, R., and McCullers, J. A. (2014) A novel cytotoxic sequence contributes to influenza A viral protein PB1-F2 pathogenicity and predisposition to secondary bacterial infection. *J. Virol.* **88,** 503–515
26. Weeks-Gorospe, J. N., Hurtig, H. R., Iverson, A. R., Schuneman, M. J., Webby, R. J., McCullers, J. A., and Huber, V. C. (2012) Naturally occurring swine influenza A virus PB1-F2 phenotypes that contribute to superinfection with Gram-positive respiratory pathogens. *J. Virol.* **86,** 9035–9043
27. Chevalier, C., Al Bazzal, A., Vidic, J., Février, V., Bourdieu, C., Bouguyon, E., Le Goffic, R., Vautherot, J. F., Bernard, J., Moudjou, M., Noinville, S., Chich, J. F., Da Costa, B., Rezaei, H., and Delmas, B. (2010) PB1-F2 influenza A virus protein adopts a β-sheet conformation and forms amyloid fibers in membrane environments. *J. Biol. Chem.* **285,** 13233–13243
28. Miodek, A., Sauriat-Dorizon, H., Chevalier, C., Delmas, B., Vidic, J., and Korri-Youssoufi, H. (2014) Direct electrochemical detection of PB1-F2 protein of influenza A virus in infected cells. *Biosens. Bioelectron* **59,** 6–13
29. Vidic, J., Le Goffic, R., Miodek, A., Bourdieu, C., Richard, C. A., Moudjou, M., Delmas, B and Chevalier, C. (2013) Detection of soluble oligomers formed by PB1-F2 influenza A virus protein *in vitro*. *J. Anal. Bioanal. Tech.* **4,** 169
30. Biancalana, M., and Koide, S. (2010) Molecular mechanism of thioflavin-T binding to amyloid fibrils. *Biochim. Biophys. Acta* **1804,** 1405–1412
31. Shai, Y. (1999) Mechanism of the binding, insertion and destabilization of phospholipid bilayer membranes by α-helical antimicrobial and cell nonselective membrane-lytic peptides. *Biochim. Biophys. Acta* **1462,** 55–70
32. Yeaman, M. R., and Yount, N. Y. (2003) Mechanisms of antimicrobial peptide action and resistance. *Pharmacol. Rev.* **55,** 27–55
33. Berridge, M. V., Herst, P. M., and Tan, A. S. (2005) Tetrazolium dyes as tools in cell biology: new insights into their cellular reduction. *Biotechnol. Annu. Rev.* **11,** 127–152
34. Miodek, A., Vidic, J., Sauriat-Dorizon, H., Richard, C. A., Le Goffic, R., Korri-Youssoufi, H., and Chevalier, C. (2014) Electrochemical detection of the oligomerization of PB1-F2 influenza A virus protein in infected cells. *Anal. Chem.* **86,** 9098–9105
35. Le Goffic, R., Leymarie, O., Chevalier, C., Rebours, E., Da Costa, B., Vidic, J., Descamps, D., Sallenave, J. M., Rauch, M., Samson, M., and Delmas, B. (2011) Transcriptomic analysis of host immune and cell death responses associated with the influenza A virus PB1-F2 protein. *PLoS Pathog.* **7,** e1002202
36. Vermes, I., Haanen, C., and Reutelingsperger, C. (2000) Flow cytometry of apoptotic cell death. *J. Immunol. Methods* **243,** 167–190
37. Zamarin, D., Ortigoza, M. B., and Palese, P. (2006) Influenza A virus PB1-F2 protein contributes to viral pathogenesis in mice. *J. Virol.* **80,** 7976–7983

38. Košík, I., Krejnusová, I., Pránovská, M., and Russ, G. (2013) The multifaceted effect of PB1-F2 specific antibodies on influenza A virus infection. *Virology* **447,** 1–8
39. Goodchild, S. C., Sheynis, T., Thompson, R., Tipping, K. W., Xue, W. F., Ranson, N. A., Beales, P. A., Hewitt, E. W., and Radford, S. E. (2014) β2-Microglobulin amyloid fibril-induced membrane disruption is enhanced by endosomal lipids and acidic pH. *PLoS ONE* **9,** e104492
40. Steunou, S., Chich, J. F., Rezaei, H., and Vidic, J. (2010) Biosensing of lipid-prion interactions: insights on charge effect, Cu(II)-ions binding and prion oligomerization. *Biosens. Bioelectron* **26,** 1399–1406
41. Swaminathan, R., Ravi, V. K., Kumar, S., Kumar, M. V., and Chandra, N. (2011) Lysozyme: a model protein for amyloid research. *Adv. Protein. Chem. Struct. Biol.* **84,** 63–111
42. Cremades, N., Cohen, S. I., Deas, E., Abramov, A. Y., Chen, A. Y., Orte, A., Sandal, M., Clarke, R. W., Dunne, P., Aprile, F. A., Bertoncini, C. W., Wood, N. W., Knowles, T. P., Dobson, C. M., and Klenerman, D. (2012) Direct observation of the interconversion of normal and toxic forms of α-synuclein. *Cell* **149,** 1048–1059
43. Daude, N., Ng, V., Watts, J. C., Genovesi, S., Glaves, J. P., Wohlgemuth, S., Schmitt-Ulms, G., Young, H., McLaurin, J., Fraser, P. E., and Westaway, D. (2010) Wild-type Shadoo proteins convert to amyloid-like forms under native conditions. *J. Neurochem.* **113,** 92–104
44. Li, Q., Chevalier, C., Henry, C., Richard, C. A., Moudjou, M., and Vidic, J. (2013) Shadoo binds lipid membranes and undergoes aggregation and fibrillization. *Biochem. Biophys. Res. Commun.* **438,** 519–525
45. Terakawa, M. S., Yagi, H., Adachi, M., Lee, Y. H., and Goto, Y. (2015) Small liposomes accelerate the fibrillation of amyloid β(1–40). *J. Biol. Chem.* **290,** 815–826
46. Domanov, Y. A., and Kinnunen, P. K. (2008) Islet amyloid polypeptide forms rigid lipid-protein amyloid fibrils on supported phospholipid bilayers. *J. Mol. Biol.* **376,** 42–54
47. Relini, A., Marano, N., and Gliozzi, A. (2014) Probing the interplay between amyloidogenic proteins and membranes using lipid monolayers and bilayers. *Adv. Colloid Interface Sci.* **207,** 81–92
48. Reynolds, N. P., Soragni, A., Rabe, M., Verdes, D., Liverani, E., Handschin, S., Riek, R., and Seeger, S. (2011) Mechanism of membrane interaction and disruption by α-synuclein. *J. Am. Chem. Soc.* **133,** 19366–19375
49. Walsh, P., Vanderlee, G., Yau, J., Campeau, J., Sim, V. L., Yip, C. M., and Sharpe, S. (2014) The mechanism of membrane disruption by cytotoxic amyloid oligomers formed by prion protein(106–126) is dependent on bilayer composition. *J. Biol. Chem.* **289,** 10419–10430
50. Bucciantini, M., Calloni, G., Chiti, F., Formigli, L., Nosi, D., Dobson, C. M., and Stefani, M. (2004) Prefibrillar amyloid protein aggregates share common features of cytotoxicity. *J. Biol. Chem.* **279,** 31374–31382
51. Bucciantini, M., Giannoni, E., Chiti, F., Baroni, F., Formigli, L., Zurdo, J., Taddei, N., Ramponi, G., Dobson, C. M., and Stefani, M. (2002) Inherent toxicity of aggregates implies a common mechanism for protein misfolding diseases. *Nature* **416,** 507–511
52. Kayed, R., Sokolov, Y., Edmonds, B., McIntire, T. M., Milton, S. C., Hall, J. E., and Glabe, C. G. (2004) Permeabilization of lipid bilayers is a common conformation-dependent activity of soluble amyloid oligomers in protein misfolding diseases. *J. Biol. Chem.* **279,** 46363–46366
53. McAuley, J. L., Tate, M. D., MacKenzie-Kludas, C. J., Pinar, A., Zeng, W., Stutz, A., Latz, E., Brown, L. E., and Mansell, A. (2013) Activation of the NLRP3 inflammasome by IAV virulence protein PB1-F2 contributes to severe pathophysiology and disease. *PLoS Pathog.* **9,** e1003392